JOURNAL OF GUIDANCE, CONTROL, AND DYNAMICS
Vol. 22, No. 1, January–February 1999

Efficient Simulation of Motions Involving Coulomb Friction

Paul C. Mitiguy*
Knowledge Revolution, San Mateo, California 94206
and
Arun K. Banerjee†
Lockheed Martin Advanced Technology Center, Palo Alto, California 94304

A realistic treatment for numerical solution of equations of motion for systems involving coulomb friction requires three sets of dynamic equations: one for sticking, one for slipping, and one for transition from sticking to slipping. An alternative treatment of stick–slip motion is described, which involves only two sets of equations, one for sticking and the other for transition and slipping. The new approach uses a single equation that continuously relates frictional forces with normal forces for both the slipping and transition phases of motion. It turns out that this equation is also capable of approximating sticking as slipping at infinitesimally small speeds, but it is computationally more efficient to use two sets of equations. The new approach is computationally efficient and is unified in the sense that when the equations of motion are cast into matrix form, the set of unknown variables is preserved during the various phases of motion (sticking, slipping, and transition), with only the last few rows of the aforementioned matrix having elements that change depending on the phase of motion. The equivalence of this new approach to the classical treatment of coulomb friction is established by comparisons of numerical results from several simulations, namely, the spin reversal of the rattleback, the effects of disturbances on a sleeping top, and the motion of a uniform sphere on a rough horizontal surface. It is shown that the same equations of motion describe the three systems for different choices of parameters.

I. Introduction

WHENEVER a point P of a body B is in contact with a surface A, there may exist a force $\boldsymbol{F}$ on P from A that may be expressed as

$$\boldsymbol{F} = \boldsymbol{N} + \boldsymbol{F}_f \tag{1}$$

where $\boldsymbol{N}$ is the component of $\boldsymbol{F}$ directed normal to the contact surface between A and B, and $\boldsymbol{F}_f$ is perpendicular to $\boldsymbol{N}$ and parallel to the contact plane. The classical kinetic coulomb friction law states that when P is slipping on A, then $\boldsymbol{F}_f$ can be written as

$$\boldsymbol{F}_f = -\mu_k |\boldsymbol{N}| \frac{{}^A\boldsymbol{v}^P}{|{}^A\boldsymbol{v}^P|} \tag{2}$$

where μ_k is an empirical constant called the coefficient of kinetic friction, $|\boldsymbol{N}|$ is the magnitude $\boldsymbol{N}$, and ${}^A\boldsymbol{v}^P$ is the velocity of P in A. Although other models for friction exist, for instance, the friction circle concept,[1] Dahl friction,[2] and viscous friction,[3] these models do not consistently provide[4] the detailed information on high-frequency chatter and the stick–slip nature of motion.

Computer simulations of motion with a classical treatment of kinetic coulomb friction encounter numerical difficulties, e.g., division by zero and numerical integration problems, whenever $|{}^A\boldsymbol{v}^P|$, the magnitude of the slipping velocity, approaches zero. One way to overcome this numerical obstacle is to check $|{}^A\boldsymbol{v}^P|$, and if it is less than ϵ_1, a small positive number, then sticking is said to occur. With a classical treatment of coulomb friction, if $|{}^A\boldsymbol{v}^P| < \epsilon_1$, one uses a second set of equations of motion because there are fewer degrees of freedom associated with the sticking motion, and $\boldsymbol{F}_f$ is no longer proportional to $|\boldsymbol{N}|$. During sticking, one must calculate the magnitude of $\boldsymbol{F}_f$ necessary to maintain sticking and test to see if $|\boldsymbol{F}_f|$ exceeds $\mu_s|\boldsymbol{N}|$, where μ_s is an empirical constant called the coefficient of static friction. If $\mu_s|\boldsymbol{N}|$ is larger than $|\boldsymbol{F}_f|$, slipping motions ensue. However, at the resumption of slipping, $|{}^A\boldsymbol{v}^P| = 0$, and Eq. (2), the coulomb kinetic friction law, fails to produce the direction of friction. A realistic treatment of coulomb friction[4–6] employs a third set of equations of motion to transition between sticking and slipping until $|{}^A\boldsymbol{v}^P|$ is larger than ϵ_2, a number slightly larger than ϵ_1. The transition friction law uses a frictional force, whose magnitude is $\mu_k|\boldsymbol{N}|$ and whose direction is identical to the direction of the static friction at the onset of slipping.

Unfortunately, the use of a classical description of the three phases of motion (sticking, slipping, and transition)[4–6] has shortcomings. It requires the derivation of three distinct sets of dynamic equations, requires relatively sophisticated logic for switching between the various phases of motion, requires good choices for ϵ_1 and ϵ_2, and renders the organization of the computer program rather cumbersome. The first objective of this paper is to show that during all phases of motion, the dynamic equations can be written as the partitioned matrix equation

$$\begin{bmatrix} W & X \\ Y & Z \end{bmatrix} \begin{bmatrix} \dot{U} \\ F \end{bmatrix} = \begin{bmatrix} Q \\ R \end{bmatrix} \tag{3}$$

where $\dot{U}$ is a column matrix of time derivatives of motion variables and F is a column matrix of contact (normal and friction) force measure numbers. It is noteworthy to mention that all of the elements of W, X, and Q and some of the elements of Y, Z, and R are independent of the phase of motion.

The second objective of this paper is to present a frictional law that successfully predicts the motion of objects that undergo both transition and slipping. This new friction law, called the continuous friction law, relates frictional forces to normal forces by two terms: the first called the slipping term and the second called the transition term,

$$\boldsymbol{F}_f = -\mu_k|\boldsymbol{N}| \frac{{}^A\boldsymbol{v}^P}{|{}^A\boldsymbol{v}^P| + \epsilon_v} - \mu_k|\boldsymbol{N}|\boldsymbol{v}_0 \frac{\epsilon_v}{|{}^A\boldsymbol{v}^P| + \epsilon_v} \tag{4}$$

$$= \frac{-\mu_k|\boldsymbol{N}|}{|{}^A\boldsymbol{v}^P| + \epsilon_v} \left({}^A\boldsymbol{v}^P + \epsilon_v \boldsymbol{v}_0\right) \tag{5}$$

where ϵ_v is a small positive number and $\boldsymbol{v}_0$ is a unit vector directed opposite the static friction forces at the onset of slipping. (Both the classical and new treatment of coulomb friction assume that the direction of impending motion is opposite the direction of static friction forces at the onset of slipping.) It will be shown that the continuous friction law successfully predicts the motion of objects that undergo both transition and slipping and is even capable (albeit inefficiently) of predicting sticking. The continuous friction law is a modification of other commonly used friction laws e.g., Ref. 7,

Received Jan. 9, 1997; revision received Dec. 2, 1997; accepted for publication June 4, 1998.

*Senior Dynamicist, Research and Development, 66 Bovet Rd.
†Consulting Scientist, Dynamics and Controls, H1-61/250. Associate Fellow AIAA.

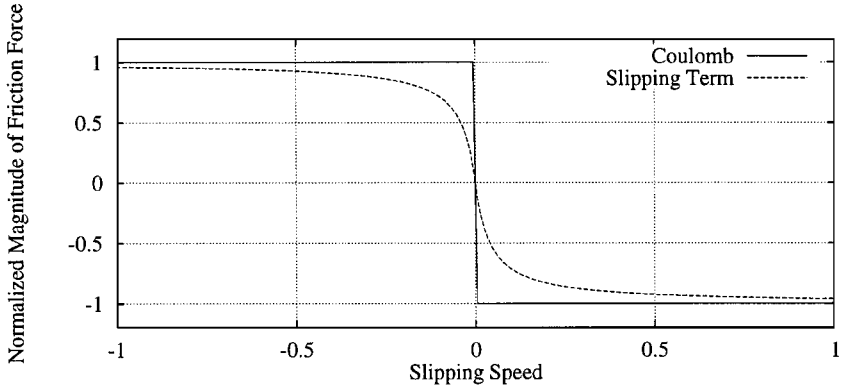

Fig. 1 Coulomb friction and slipping term of continuous friction.

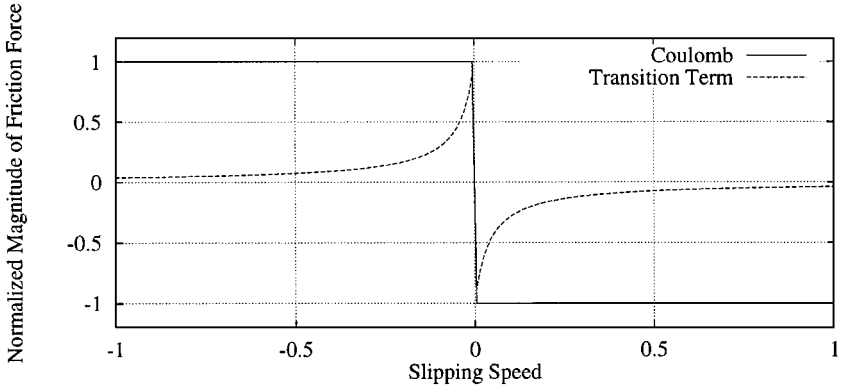

Fig. 2 Coulomb friction and transition term of continuous friction.

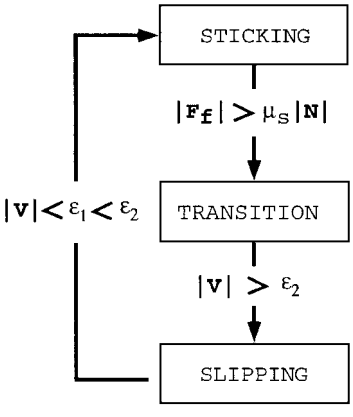

Fig. 3 Kane and Levinson[6] flow chart.

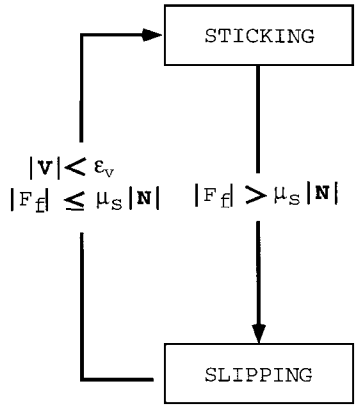

Fig. 4 New flow chart.

which use an ϵ_v to avoid the singularities in the coulomb kinetic friction law. Each of the two terms in the continuous friction law, Eq. (4), is shown graphically in Figs. 1 and 2, when $\epsilon_v = 0.04$. The effect of ϵ_v on simulation speed and accuracy has not been well documented. Thus, one objective of this paper is to document its role.

To demonstrate the validity of the new friction formulations, certain classical problems involving friction, namely, the spin reversal of the rattleback, the effects of disturbances on a sleeping top, and the motion of a uniform sphere on a rough horizontal surface, are examined.

Finally, two methods for improving simulation speed are presented.

II. Comparison of Classical and New Treatment of Coulomb Friction

By using the continuous friction law in conjunction with the unified friction formulation, much of the complexity of classical numerical solutions of coulomb friction can be avoided. For example, by using the continuous friction law to simulate both the transition and slipping phases of motion, the switching logic presented in Ref. 6 can be substantially simplified. The differences in the switching logic used by Kane and Levinson[6] with the new logic is shown graphically in Figs. 3 and 4. The switching logic advocated in Ref. 6 is summarized as follows.

1) Sticking friction: Solve for τ_1, the magnitude of the normal force, and τ_2 and τ_3, the measure numbers of the static friction force. Calculate $|\boldsymbol{F}_f| = \sqrt{(\tau_2^2 + \tau_3^2)}$, the magnitude of the friction force. If $|\boldsymbol{F}_f| \geq \mu_s \tau_1$, form the unit vector $\boldsymbol{v}_0$, which is directed opposite the static friction force, and switch to transition friction.

2) Transition friction: Apply a friction force $\boldsymbol{F}_f = -\mu_k \tau_1 \boldsymbol{v}_0$. Calculate $|\boldsymbol{v}|$, the magnitude of the velocity of the contact point, i.e., the slipping velocity. If $|\boldsymbol{v}| > \epsilon_2$, where ϵ_2 is a somewhat arbitrary positive number, switch to slipping friction.

3) Slipping friction: Apply a friction force $\boldsymbol{F}_f = -\mu_k \tau_1 \boldsymbol{v}/|\boldsymbol{v}|$. If $|\boldsymbol{v}| \leq \epsilon_1$, where $0 < \epsilon_1 < \epsilon_2$, switch to sticking friction.

The new switching logic for the sticking phase is identical to that presented in Ref. 6, but the rest of the logic is substantially simpler.

1) Sticking friction: Solve for τ_1, τ_2, and τ_3. Calculate $|\boldsymbol{F}_f| = \sqrt{(\tau_2^2 + \tau_3^2)}$. If $|\boldsymbol{F}_f| > \mu_s \tau_1$, form $\boldsymbol{v}_0$ and switch to the continuous friction law.

2) Continuous friction: Apply a friction force $\boldsymbol{F}_f = -\mu_k \tau_1 [(\boldsymbol{v} + \epsilon_v \boldsymbol{v}_0)/(|\boldsymbol{v}| + \epsilon_v)]$, where ϵ_v is a small positive number. If $|\boldsymbol{v}| > \epsilon_v$ and the integration is on a boundary, set $\boldsymbol{v}_0 = 0$, removing the transition term of the continuous friction law. (By integration boundary, we mean any place in the integration process where the integration is self-starting and, thus, can handle discontinuities in forces and/or motion.) If $|\boldsymbol{v}| < \epsilon_v$ and $|\boldsymbol{F}_f| > \mu_s \tau_1$, switch to sticking friction.

The new switching logic has several other improvements over the logic in Ref. 6. In Ref. 6, switching between various phases of motion occur only at user-specified integration time steps. To desensitize the simulation results from the user-specified integration step, it is better to allow instead switching at all integration boundaries.

It is clear that using the continuous friction law substantially reduces the complexity in the switching logic. The unified friction formulation provides additional benefits. In Ref. 6, the simulation requires the derivation of three distinct sets of dynamic equations with the number of variables being integrated changing with changes in the phase of motion. The unified friction formulation eliminates the need to change the number of variables being integrated and requires only minor changes to the Y, Z, and R matrices in Eq. (3) to switch between phases. One major advantage of the formulation in Ref. 6 is that a minimal set of dynamic equations are produced for each phase of motion. Some of the inefficiencies found in the unified friction formulation are removed by using the methods advocated in Sec. VI.

III. Spin Reversal of the Rattleback

The rattleback, also called a celt or wobblestone, is a boat-shaped object, which, when placed on a rough horizontal surface and rotated about a vertical axis, sometimes stops rotating, begins to oscillate, then starts rotating in the reverse direction. This problem has attracted the attention of many eminent dynamicists[5,8–11] with Hubbard and Garcia[5] providing both theoretical and experimental results. It will be shown how the unified friction formulation [Eq. (3)] and the continuous friction law [Eq. (5)] may be applied to simulate the spin reversal of a rattleback.

Although the equations of motion of the rattleback have been presented before, the authors believe that the derivation of the equations presented is instructive, concise, and novel in its solution of the contact surface conditions. Figure 5 is a schematic representation of a rattleback B in contact with a rough horizontal surface N at point B_n of B. The surface S of B is an ellipsoid whose axes S_1, S_2, S_3 intersect at point S_0 on B. The locus of points on S is defined by the equation

$$f(s_1, s_2, s_3) = \left(s_1^2/a^2\right) + \left(s_2^2/b^2\right) + \left(s_3^2/c^2\right) - 1 = 0 \qquad (6)$$

where s_i are the S_i $(i = 1, 2, 3)$ coordinates of a generic point P on S, and a, b, and c are semidiameters of the ellipsoid. The mass of B is M, and B_0, the mass center of B, lies on S_1, a distance h from S_0. The nonzero central inertia scalars of B corresponding to lines parallel to S_1, S_2, and S_3 are I_{11}, I_{22}, I_{33}, and I_{23}, respectively. In other words, S_1 is a central principal axis of inertia, whereas S_2 and S_3 are not.

In formulating equations of motion, it is convenient to introduce dextral sets of mutually perpendicular unit vectors $\boldsymbol{b}_i$ and $\boldsymbol{n}_i$ $(i = 1, 2, 3)$, fixed in B and N, respectively, with $\boldsymbol{b}_i$ parallel to S_i $(i = 1, 2, 3)$, and $\boldsymbol{n}_1$ directed vertically upward and perpendicular to the planar surface of N in contact with B. The orientation of B in N is found by first aligning $\boldsymbol{b}_i$ with $\boldsymbol{n}_i$ $(i = 1, 2, 3)$, and then subjecting B to the body-fixed rotation sequence described in magnitude and direction by $q_1\boldsymbol{b}_1$, $q_2\boldsymbol{b}_2$, and $q_3\boldsymbol{b}_3$. The elements of the direction cosine matrix C_{ij} $(i, j = 1, 2, 3)$ defined as

$$C_{ij} \triangleq \boldsymbol{n}_i \cdot \boldsymbol{b}_j \qquad (i, j = 1, 2, 3) \qquad (7)$$

which arise from this rotation sequence, are given by

$$C = \begin{bmatrix} \cos q_2 \cos q_3 & -\sin q_3 \cos q_2 & \sin q_2 \\ \sin q_3 \cos q_1 + \sin q_1 \sin q_2 \cos q_3 & \cos q_1 \cos q_3 - \sin q_1 \sin q_2 \sin q_3 & -\sin q_1 \cos q_2 \\ \sin q_1 \sin q_3 - \sin q_2 \cos q_1 \cos q_3 & \sin q_1 \cos q_3 + \sin q_2 \sin q_3 \cos q_1 & \cos q_1 \cos q_2 \end{bmatrix} \qquad (8)$$

The two parameters used in Ref. 10 to characterize the orientation of B in N are the spin angle q_1 and the wobble angle δ, defined as

$$\delta \triangleq \arccos(\boldsymbol{n}_1 \cdot \boldsymbol{b}_1) = \arccos(C_{11}) \qquad (9)$$

Before proceeding with a dynamic analysis, we note that the s_i $(i = 1, 2, 3)$ coordinates of B_n relative to S_0 can be found from the fact that the normal to S is parallel to $\boldsymbol{n}_1$ and B_n must lie along the surface of N. Because $\nabla f(s_1, s_2, s_3)$, the gradient to the rattleback's curved surface, is parallel to the normal of S, one can write

$$\nabla f(s_1, s_2, s_3) = 2\lambda \boldsymbol{n}_1 \qquad (10)$$

where λ is a scalar quantity that will be determined presently. After making use of Eq. (6) to calculate $\nabla f(s_1, s_2, s_3)$, and substituting into Eq. (10) and simplifying, one arrives at

$$\left(s_1/a^2\right)\boldsymbol{b}_1 + \left(s_2/b^2\right)\boldsymbol{b}_2 + \left(s_3/c^2\right)\boldsymbol{b}_3 = \lambda \boldsymbol{n}_1 \qquad (11)$$

Dot multiplication of Eq. (11) with $\boldsymbol{b}_1$, $\boldsymbol{b}_2$, and $\boldsymbol{b}_3$ produces

$$s_1 = a^2 C_{11} \lambda \qquad (12)$$

$$s_2 = b^2 C_{12} \lambda \qquad (13)$$

$$s_3 = c^2 C_{13} \lambda \qquad (14)$$

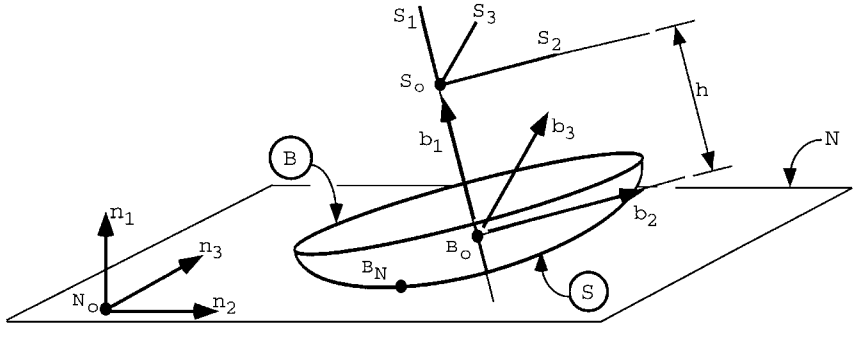

Fig. 5 Rattleback.

Substituting Eqs. (12–14) into Eq. (6) and solving for λ produces

$$\lambda = -\frac{1}{\sqrt{(aC_{11})^2 + (bC_{12})^2 + (cC_{13})^2}} \tag{15}$$

To describe the motion of B in N, the motion variables u_i ($i = 1, 2, 3$) are defined as the $\boldsymbol{b}_1$, $\boldsymbol{b}_2$, and $\boldsymbol{b}_3$ measure numbers of the angular velocity of B in N as

$$u_1 \triangleq \boldsymbol{\omega} \cdot \boldsymbol{b}_1, \qquad u_2 \triangleq \boldsymbol{\omega} \cdot \boldsymbol{b}_2, \qquad u_3 \triangleq \boldsymbol{\omega} \cdot \boldsymbol{b}_3 \tag{16}$$

and the motion variables u_i ($i = 4, 5, 6$) are defined as the $\boldsymbol{n}_1$, $\boldsymbol{n}_2$, and $\boldsymbol{n}_3$ measure numbers of the velocity of B_0 in N as

$$u_4 \triangleq \boldsymbol{v}^{B_0} \cdot \boldsymbol{n}_1, \qquad u_5 \triangleq \boldsymbol{v}^{B_0} \cdot \boldsymbol{n}_2, \qquad u_6 \triangleq \boldsymbol{v}^{B_0} \cdot \boldsymbol{n}_3 \tag{17}$$

With the definitions of u_i ($i = 1, 2, 3$) given in Eq. (16) and the description of the orientation of B in N in terms of q_i ($i = 1, 2, 3$), the kinematic differential equation for q_i may be written as

$$\dot{q}_1 = \frac{(u_1 \cos q_3 - u_2 \sin q_3)}{\cos q_2} \tag{18}$$

$$\dot{q}_2 = (u_1 \sin q_3 + u_2 \cos q_3) \tag{19}$$

$$\dot{q}_3 = (-u_1 \cos q_3 + u_2 \sin q_3) \tan q_2 + u_3 \tag{20}$$

The relevant forces that act on B are a gravitational force, whose line of action passes through B_0, given by

$$\boldsymbol{F}^{B_0} = -Mg\boldsymbol{n}_1 \tag{21}$$

and a contact force acting at B_n, the point of B in contact with N, given by

$$\boldsymbol{F}^{B_n} = \tau_1 \boldsymbol{n}_1 + \tau_2 \boldsymbol{n}_2 + \tau_3 \boldsymbol{n}_3 \tag{22}$$

Note that we have not assumed any particular relationship between the tangential (frictional) components and normal component of the contact force. Also, note that there are six motion variables, $u_1, \ldots, u_6$, whereas there are only five degrees of freedom when B is slipping on N and only three when B rolls on N. The extra motion variable(s) will be used to get equations governing the value of τ_1, the normal component of the contact force, and during sticking (rolling), the values of τ_2 and τ_3, the tangential components of the contact force.

The Newton–Euler equations of motion of the rattleback are

$$\boldsymbol{p}^{B_0 B_n} \times \boldsymbol{F}^{B_n} = \underline{\boldsymbol{I}} \cdot \boldsymbol{\alpha} + \boldsymbol{\omega} \times \underline{\boldsymbol{I}} \cdot \boldsymbol{\omega} \tag{23}$$

$$\boldsymbol{F}^{B_0} + \boldsymbol{F}^{B_n} = M\boldsymbol{a}^{B_0} \tag{24}$$

where $\underline{\boldsymbol{I}}$ is the central inertia dyadic of B, $\boldsymbol{\alpha}$ is the angular acceleration of B in N, and $\boldsymbol{p}^{B_0 B_n}$ is the position vector from B_0 to B_n.

To Eqs. (23) and (24), one must append the constraint equation that enforces the condition that the normal component of the velocity of B_n is always zero, i.e.,

$$\boldsymbol{v}^{B_n} \cdot \boldsymbol{n}_1 = (s_2 C_{13} - s_3 C_{12})u_1 + [s_3 C_{11} - (h + s_1)C_{13}]u_2 + [-s_2 C_{11} + (h + s_1)C_{12}]u_3 + u_4 = 0 \tag{25}$$

Furthermore, when the body is sticking (rolling), two additional constraint equations are required. These equations enforce the condition that the tangential components of the velocity of B_n are zero, namely,

$$\boldsymbol{v}^{B_n} \cdot \boldsymbol{n}_2 = (s_2 C_{23} - s_3 C_{22})u_1 + [s_3 C_{21} - (h + s_1)C_{23}]u_2 + [-s_2 C_{21} + (h + s_1)C_{22}]u_3 + u_5 = 0 \tag{26}$$

$$\boldsymbol{v}^{B_n} \cdot \boldsymbol{n}_3 = (s_2 C_{33} - s_3 C_{32})u_1 + [s_3 C_{31} - (h + s_1)C_{33}]u_2 + [-s_2 C_{31} + (h + s_1)C_{32}]u_3 + u_6 = 0 \tag{27}$$

Of course, the equations of motion depend on whether the rattleback is sticking (rolling), slipping, or undergoing transition from sticking to slipping. One premise of this paper is to show that during all phases of motion, the dynamic equations can be written as the partitioned matrix equation

$$\begin{bmatrix} W & X \\ Y & Z \end{bmatrix} \begin{bmatrix} \dot{U} \\ F \end{bmatrix} = \begin{bmatrix} Q \\ R \end{bmatrix} \tag{28}$$

where, for the rattleback, W is a 6×6 mass matrix, X is a 6×3 matrix, Y is a 3×6 matrix, Z is a 3×3 matrix, Q is a 6×1 column matrix, and R is a 3×1 column matrix, and $\dot{U}$ and F are defined as

$$\dot{U} = \begin{bmatrix} \dot{u}_1 \\ \vdots \\ \dot{u}_6 \end{bmatrix}, \qquad F = \begin{bmatrix} \tau_1 \\ \tau_2 \\ \tau_3 \end{bmatrix} \tag{29}$$

The elements of the W, X, and Q matrices are independent of the phase of motion and are generated by dot multiplication of Eq. (23) with $\boldsymbol{b}_1$, $\boldsymbol{b}_2$, and $\boldsymbol{b}_3$, and by dot multiplication of Eq. (24) with $\boldsymbol{n}_1$, $\boldsymbol{n}_2$, and $\boldsymbol{n}_3$. The matrices W, X, and Q may be written

$$W = \begin{bmatrix} I_{11} & 0 & 0 & 0 & 0 & 0 \\ 0 & I_{22} & I_{23} & 0 & 0 & 0 \\ 0 & I_{23} & I_{33} & 0 & 0 & 0 \\ 0 & 0 & 0 & M & 0 & 0 \\ 0 & 0 & 0 & 0 & M & 0 \\ 0 & 0 & 0 & 0 & 0 & M \end{bmatrix} \tag{30}$$

$$X = \begin{bmatrix} s_3 C_{12} - s_2 C_{13} & s_3 C_{22} - s_2 C_{23} & s_3 C_{32} - s_2 C_{33} \\ -s_3 C_{11} + (h + s_1)C_{13} & -s_3 C_{21} + (h + s_1)C_{23} & -s_3 C_{31} + (h + s_1)C_{33} \\ s_2 C_{11} - (h + s_1)C_{12} & s_2 C_{21} - (h + s_1)C_{22} & s_2 C_{31} - (h + s_1)C_{32} \\ -1 & 0 & 0 \\ 0 & -1 & 0 \\ 0 & 0 & -1 \end{bmatrix} \tag{31}$$

$$Q = \begin{bmatrix} I_{22}u_2u_3 + I_{23}u_3^2 - I_{23}u_2^2 - I_{33}u_2u_3 \\ -u_1(I_{11}u_3 - I_{23}u_2 - I_{33}u_3) \\ u_1(I_{11}u_2 - I_{22}u_2 - I_{23}u_3) \\ -Mg \\ 0 \\ 0 \end{bmatrix} \tag{32}$$

In general, the matrices Y, Z, and R appearing in Eq. (28) are dependent on the phase of motion, i.e., sticking, slipping, or transition. However, the first row of Y, Z, and R results from time differentiation of Eq. (25), the normal contact condition, and is independent of the phase of motion. The nonzero elements of the first row of Y, Z, and R are

$$Y_{11} = s_2 C_{13} - s_3 C_{12} \tag{33}$$

$$Y_{21} = s_3 C_{11} - (h + s_1)C_{13} \tag{34}$$

$$Y_{31} = -s_2 C_{11} + (h + s_1) C_{12} \tag{35}$$

$$Y_{14} = 1 \tag{36}$$

$$\begin{aligned} R_1 = {} & [C_{11}\dot{s}_2 + s_2\dot{c}_{11} - C_{12}\dot{s}_1 - (h + s_1)\dot{c}_{12}]u_3 \\ & - (C_{13}\dot{s}_2 + s_2\dot{c}_{13} - C_{12}\dot{s}_3 - s_3\dot{c}_{12})u_1 \\ & - [C_{11}\dot{s}_3 + s_3\dot{c}_{11} - C_{13}\dot{s}_1 - (h + s_1)\dot{c}_{13}]u_2 \end{aligned} \tag{37}$$

The last two rows of Eq. (28) depend on whether the rattleback is sticking, slipping, undergoing transition, or subject to the continuous friction law. The next sections give the elements of Y, Z, and R for each of the various phases of motion.

A. Sticking (Rolling) Friction

Referring to Eq. (28), the nonzero elements of the last two rows of Y, Z, and R that result from time differentiation of Eqs. (26) and (27), the rolling (sticking) contact condition, are

$$Y_{21} = s_2 C_{23} - s_3 C_{22} \tag{38}$$

$$Y_{22} = s_3 C_{21} - (h + s_1) C_{23} \tag{39}$$

$$Y_{23} = -s_2 C_{21} + (h + s_1) C_{22} \tag{40}$$

$$Y_{25} = 1 \tag{41}$$

$$Y_{31} = s_2 C_{33} - s_3 C_{32} \tag{42}$$

$$Y_{32} = s_3 C_{31} - (h + s_1) C_{33} \tag{43}$$

$$Y_{33} = -s_2 C_{31} + (h + s_1) C_{32} \tag{44}$$

$$Y_{36} = 1 \tag{45}$$

$$\begin{aligned} R_2 = {} & [C_{21}\dot{s}_2 + s_2\dot{c}_{21} - C_{22}\dot{s}_1 - (h + s_1)\dot{c}_{22}]u_3 \\ & - (C_{23}\dot{s}_2 + s_2\dot{c}_{23} - C_{22}\dot{s}_3 - s_3\dot{c}_{22})u_1 \\ & - [C_{21}\dot{s}_3 + s_3\dot{c}_{21} - C_{23}\dot{s}_1 - (h + s_1)\dot{c}_{23}]u_2 \end{aligned} \tag{46}$$

$$\begin{aligned} R_3 = {} & [C_{31}\dot{s}_2 + s_2\dot{c}_{31} - C_{32}\dot{s}_1 - (h + s_1)\dot{c}_{32}]u_3 \\ & - (C_{33}\dot{s}_2 + s_2\dot{c}_{33} - C_{32}\dot{s}_3 - s_3\dot{c}_{32})u_1 \\ & - [C_{31}\dot{s}_3 + s_3\dot{c}_{31} - C_{33}\dot{s}_1 - (h + s_1)\dot{c}_{33}]u_2 \end{aligned} \tag{47}$$

While the rattleback is rolling, a concomitant condition for τ_1, τ_2, and τ_3 must be satisfied, namely,

$$\sqrt{\tau_2^2 + \tau_3^2} \le \mu_s \tau_1 \tag{48}$$

B. Transition and Slipping Friction

Transition from sticking to slipping occurs the instant when the inequality condition in Eq. (48) is no longer satisfied. Denoting the values of τ_2 and τ_3 at this instant as $\hat{\tau}_2$ and $\hat{\tau}_3$, respectively, the direction of impending motion $\boldsymbol{v}_0$ is classically assumed[6] to be

$$\boldsymbol{v}_0 = -\frac{\hat{\tau}_2 \boldsymbol{n}_2 + \hat{\tau}_3 \boldsymbol{n}_3}{|\hat{\tau}_2 \boldsymbol{n}_2 + \hat{\tau}_3 \boldsymbol{n}_3|} \tag{49}$$

and the continuous friction law, Eq. (5), leads to

$$\tau_2 \boldsymbol{n}_2 + \tau_3 \boldsymbol{n}_3 = -\mu_k \tau_1 \frac{\boldsymbol{v}^{B_n} + \epsilon_v \boldsymbol{v}_0}{|\boldsymbol{v}^{B_n}| + \epsilon_v} \tag{50}$$

Referring to Eq. (28), one sees that the nonzero elements of the last two rows of Y, Z, and R that result from Eq. (50) are

$$Z_{21} = \mu_k \frac{\left(\boldsymbol{v}^{B_n} + \epsilon_v \boldsymbol{v}_0\right) \cdot \boldsymbol{n}_2}{|\boldsymbol{v}^{B_n}| + \epsilon_v} \tag{51}$$

$$Z_{22} = 1 \tag{52}$$

$$Z_{31} = \mu_k \frac{\left(\boldsymbol{v}^{B_n} + \epsilon_v \boldsymbol{v}_0\right) \cdot \boldsymbol{n}_3}{|\boldsymbol{v}^{B_n}| + \epsilon_v} \tag{53}$$

$$Z_{33} = 1 \tag{54}$$

Thus, it has been shown that the three phases of motion (sticking, transition, and slipping) can be handled in the format of Eq. (28), changing only the contents of the second and third rows of the matrices Y, Z, and R. The particular forms of Y, Z, and R depend on the satisfaction of specific tests for sticking or transition and slipping.

C. Simulation Results: Rattleback

Numerical results based on both the unified friction formulation and the continuous friction law were generated for the same rattleback considered in Ref. 10, that is, a simulation was performed with the constants $g = 9.81$ m/s^2, $a = 0.02$ m, $b = 0.2$ m, $c = 0.03$ m, $h = 0.01$ m, $M = 1$ kg, $I_{11} = 1.7 \times 10^{-3}$ kg-m^2, $I_{22} = 2.0 \times 10^{-4}$ kg-m^2, $I_{33} = 1.6 \times 10^{-3}$ kg-m^2, and $I_{23} = 2.0 \times 10^{-5}$ kg-m^2 and the initial values $q_1 = 0$ deg, $q_2 = 0.5$ deg, $q_3 = -0.5$ deg, $u_1 = 5$ rad/s, $u_2 = u_3 = 0$, $u_4 = 0.0007415$ m/s, $u_5 = -0.001956$ m/s, and $u_6 = 0.08693$ m/s. The initial values for u_4, u_5, and u_6 correspond to an initial rolling condition. Numerical integration was performed for 5 s with a fourth-order, variable-step, Kutta–Merson integrator with an integration step of 0.01 s, and an absolute and relative error tolerance of 1.0×10^{-7}.

Figures 6 and 7 show time histories for the spin angle q_1 and the wobble angle δ when the surface between N and B has friction coefficients of $\mu_k = \mu_s = 0.8$, values that are sufficiently high to ensure continuous sticking (rolling). The solid lines result from using the unified friction formulation in conjunction with the continuous friction law and exactly match the results found in Ref. 10.

Remark: Effects of ϵ_v on simulation speed and accuracy. The quantity ϵ_v that appears in Eq. (5) can have a profound effect on simulation speed and accuracy if one does not use the unified friction formulation. It has been well known that without the unified friction formulation, small values of ϵ_v lead to stiff slow numerical

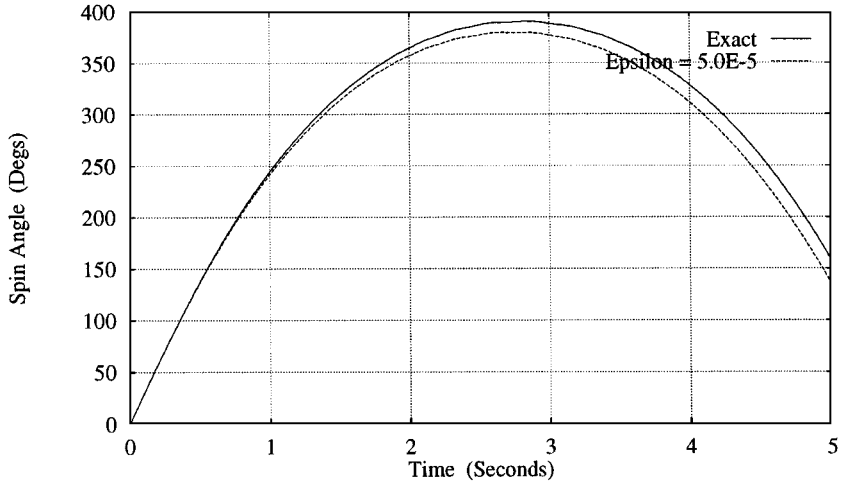

Fig. 6 Time history of spin angle q_1 showing spin reversal.

integration, whereas large values of ϵ_v yield inaccurate results. For example, the dotted lines in Figs. 6 and 7 are the simulation results found by using solely Eq. (5), the continuous friction law, with $\epsilon_v = 5.0 \times 10^{-5}$. These results demonstrate the claim that the continuous friction law, which treats sticking as slipping at infinitesimally small speeds, can approximate sticking (rolling). The continuous friction law predicts the spin reversal of the rattleback more accurately with $\epsilon_v = 1.0 \times 10^{-5}$; however, the simulation proceeds very slowly. Because the continuous friction law approximates sticking by slipping at infinitesimally small speeds, it is not surprising that it takes significantly longer to simulate than the equations that exactly describe the sticking condition. For example, to simulate the 5 s of motion shown in Figs. 6 and 7, high-precision numerical integration was performed with a fourth-order, Kutta–Merson, variable time-step integrator with a maximum integration step of 0.01 s and error tolerances of 1.0×10^{-7} on an AST Powerexec, 33 MHz computer. To generate the data took only 5 min when using the unified friction formulation (the exact rolling equations) but well over 6 h when using the continuous friction law with $\epsilon_v = 1.0 \times 10^{-5}$ and only the dynamical equations for slipping.

Table 1 Rattleback: effect of ϵ_v on simulation speed and accuracy

ϵ_v	Spin angle, deg	Number of calls	Simulation time, min
1.0×10^{-3}	− 8.47	287,491	16.8
1.0×10^{-4}	−116.18	1,051,651	80.0
5.0×10^{-5}	−134.81	1,707,426	99.5
1.0×10^{-5}	−152.32	6,798,331	396.0
Rolling	−157.57	90,491	4.3

The role that ϵ_v plays in simulation accuracy and speed is simple. Smaller values of ϵ_v result in more accurate, slower simulations than larger values of ϵ_v. To quantify this statement, Table 1 shows the value of q_1 at $t = 5$ s, the number of function calls made by the numerical integrator, and the time required to perform numerical integration, for various values of ϵ_v. At the bottom of Table 1, a precise value of q_1, obtained by integrating the exact rolling equations, is shown.

IV. Dynamic Analysis of a Sleeping Top

The dynamic analysis of a symmetric top has received a tremendous amount of attention, e.g., Refs. 6 and 12–20. Most analyses make certain simplifying assumptions such as a contact plane that is perfectly smooth (no friction) or a rough contact plane that prevents slipping from occurring. Few analyses included transitions from slipping to rolling and vice versa because no closed-form analytical expressions for the general motion exist. In this section, it is shown how the unified friction formulation [Eq. (3)] in conjunction with the continuous friction law [Eq. (5)] may be applied to efficiently simulate the motion of a sleeping top, see Fig. 8.

Because the equations of motion developed for the rattleback also govern the motion of the symmetric top, only the initial values for q_i $(i = 1, 2, 3)$ and u_i $(i = 1, 2, \ldots, 5)$ and the constants that describe the geometry and mass distribution of the rattleback need to be changed to simulate the top. To compare numerical results with those availiable in the literature,[6] the following values were chosen: $g = 9.81$ m/s^2, $\mu_k = 0.009$, $\mu_s = 0.01$, $a = b = c = 0.01$ m, $h = -0.005$ m, $M = 1$ kg, $I_{11} = 5.0 \times 10^{-6}$ kg-m^2, $I_{22} = 7.0 \times 10^{-6}$ kg-m^2, $I_{33} = 7.0 \times 10^{-6}$ kg-m^2, $I_{23} = 0$, $q_1 = q_2 = q_3 = 0$ deg, $u_1 = 43.94$ rad/s, $u_2 = 0.087$ rad/s, $u_3 = u_4 = u_5 = 0$, and $u_6 =$

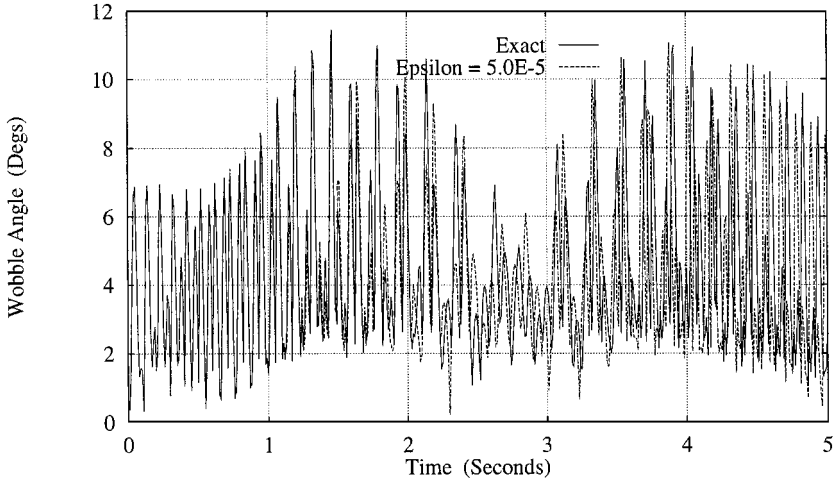

Fig. 7 Time history of wobble angle δ.

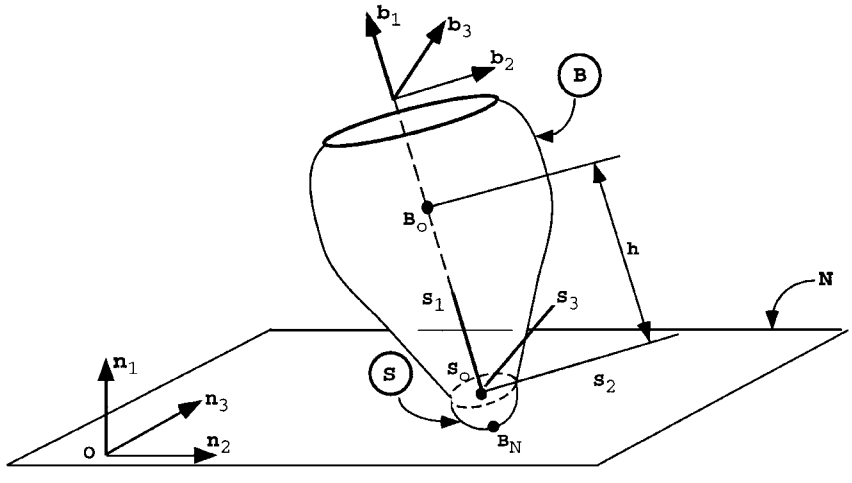

Fig. 8 Sleeping top.

-6.45×10^{-4} m/s. The initial values for u_4, u_5, and u_6 correspond to an initial sticking condition, namely, $\boldsymbol{v}^{B_n} = 0$. Numerical integration was performed for 2 s with a fourth-order, Kutta–Merson integrator with an integration step of 0.01 s, with an absolute and relative error tolerance of 1.0×10^{-7}, and with $\epsilon_v = 1.0 \times 10^{-5}$.

Figure 9 shows the time history of the inclination angle δ. These results agree with those presented in Ref. 6. The first curve in Fig. 9 shows that the sleeping top will turn over, if it is subjected to a large perturbation, which in this example is assigning u_2 an initial value of 0.087 rad/s. The second curve shows that if the perturbation is reduced by half ($u_2 = 0.043$ rad/s), the top does not turn over. The third curve shows that if the perturbation is again reduced by half, ($u_2 = 0.022$ rad/s) the inclination angle is nearly halved. The algorithm in Ref. 6 uses three sets of dynamic equations, one for sticking (rolling), one for slipping, and one for transition. Because of the three sets of dynamic equations, the algorithm in Ref. 6 requires fairly complex logic for switching sets at various points in the simulation. The algorithm used to generate Fig. 9 uses only two sets of dynamic equations, one for sticking (rolling) and the other for transition and slipping, and the switching logic is simple.

Remark: Effects of ϵ_v on simulation speed and accuracy. In Sec. III.C, it was shown the value assigned to ϵ_v had a profound effect on simulation speed and accuracy if one did not employ the unified friction formulation. If instead, one chooses to employ the unified friction formulation in conjunction with the continuous friction law [Eq. (5)], the effect of ϵ_v on simulation speed and accuracy is minor. To quantify the last statement, Table 2 shows the value of the inclination angle δ at $t = 2$ s, the number of function calls made by the numerical integrator, and the time required to perform numerical integration, for various values of ϵ_v. As is evident from Table 2, smaller values of ϵ_v do not correspond to more function calls (or slower simulation times) when one uses the unified friction formulation to switch between the continuous friction law and the sticking (rolling) equations. However, smaller values of ϵ_v do result in more accurate simulation results.

Table 2 Sleeping top: effect of ϵ_v on simulation speed and accuracy

ϵ_v	Inclination angle, deg	Number of calls
1.0×10^{-1}	127.33	26,491
1.0×10^{-3}	118.89	26,838
1.0×10^{-5}	114.67	25,936
1.0×10^{-7}	114.59	25,996

V. Slip–Stick Motions of a Homogenous Sphere

Although there are no closed-form solutions available for general motions of the rattleback or sleeping top, there are closed-form solutions available[21,22] for the motion of a uniform sphere (see Fig. 10) that transitions from slipping to rolling on a rough horizontal plane. These closed-form solutions can be used to assess the speed and accuracy of the unified friction formulation and the continuous friction law.

By choosing appropriate geometric and mass distribution parameters, the same equations of motion developed for the rattleback can be used to simulate the motion of a sphere on a rough horizontal plane. The following values were chosen: $g = 9.81$ m/s^2, $\mu_k = 0.3$, $\mu_s = 0.33$, $a = b = c = 1.0$ m, $h = 0$, $M = 1$ kg, $I_{11} = I_{22} = I_{33} = 0.4$ kg-m^2, $I_{23} = 0$, $q_1 = q_2 = q_3 = 0$ deg, $u_2 = -7.0$ rad/s, $u_5 = 5.0$ m/s, $u_1 = u_3 = u_4 = u_6 = 0$. Numerical integration was performed for 1.0 s with a fourth-order Kutta–Merson integrator with an integration step of 0.001 s and an absolute and relative error tolerance of 1.0×10^{-7}. To minimize the effect of ϵ_v on

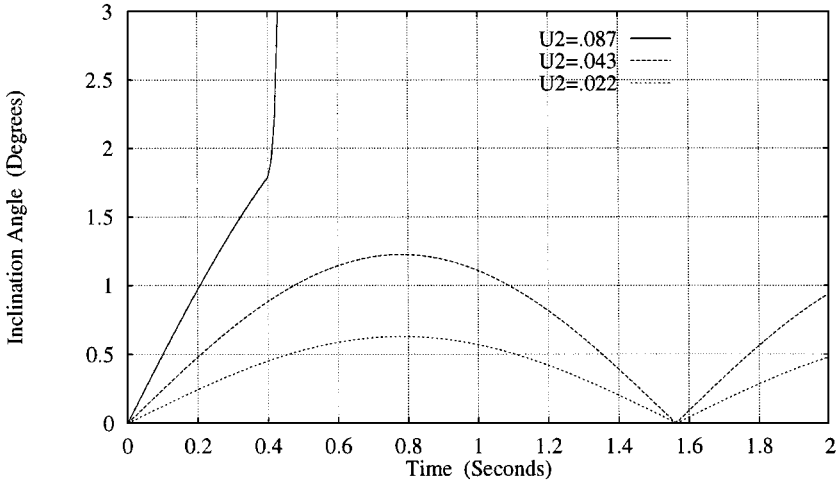

Fig. 9 Effects of disturbances on a sleeping top.

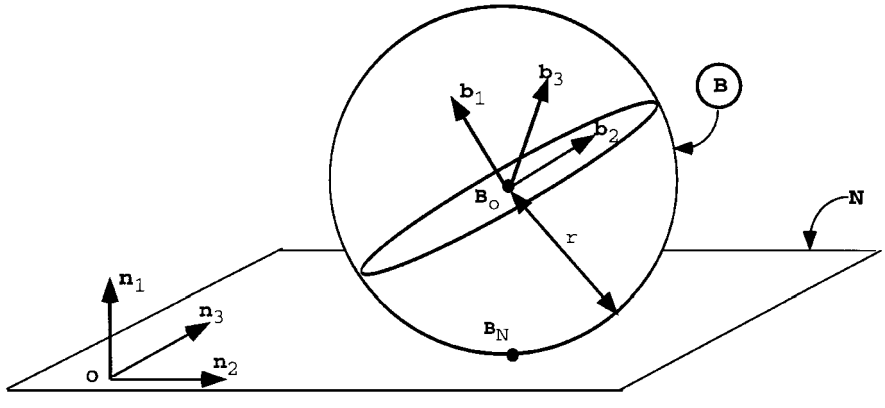

Fig. 10 Homogenous sphere.

simulation speed and accuracy, the unified friction formulation was used with two sets of dynamic equations: one for sticking (rolling) and the continuous friction law for transition and slipping. The motion traced out on the plane by the contact point is shown in Fig. 11. The solid line shows the exact solution, whereas the various dotted lines show the numerical solutions for various values of ϵ_v. As is apparent in Fig. 11, the effect of ϵ_v on simulation accuracy is minor, even when relatively large values of ϵ_v are used.

Remark: Effects of ϵ_v on simulation speed and accuracy. To see the effect of ϵ_v on simulation accuracy and speed, consider Table 3, which shows the percentage error in time to transition from slipping to rolling, that is, the duration of time that slipping persists, and the number of function calls made by the numerical integrator. As is apparent in Table 3, an order of magnitude decrease in ϵ_v results in approximately an order of increase in simulation accuracy. Because the unified friction formulation is employed, the number of calls made by the integrator (and thus the simulation speed) is only minimally affected by small values of ϵ_v.

VI. Improving Simulation Speed

The unified friction formulation, Eq. (3), provides a convenient mechanism to simulate coulomb friction. However, with some minor algebraic manipulations, the number of linear equations being solved at each time step can be reduced. For example, during transition and slipping, one may make a simple substitution for the friction force that reduces the number of coupled linear equations from nine to seven, effectively halving the number of operations required to solve the linear system. (The number of operations required to solve a coupled set of linear equations varies with the number of equations cubed.) During sticking, one may use Kane's method to split the work of uncoupling the linear equations from one set of nine equations to three sets of three equations.

A. Substituting for the Friction Force

Whenever slipping is occurring, the size of the set of linear equations can be reduced without loss of precision. This is accomplished by solving the equation(s) that relate the friction force to the normal force, eliminating the friction force measure numbers from the list of unknowns, and reflecting this solution into the elements of the X matrix. For example, for the rattleback, this process is carried out by solving for τ_2 and τ_3 in terms of τ_1, eliminating τ_2 and τ_3 from the list of unknowns, and modifying the elements of the X matrix to

$$X_{i1} = X_{i1} - X_{i2}Z_{21} - X_{i3}Z_{31} \qquad (i = 1, \ldots, 6) \tag{55}$$

After solving for $\dot{u}_1, \ldots, \dot{u}_6$, updated values for τ_2 and τ_3 are computed as

$$\tau_2 = -Z_{21}\tau_1 \tag{56}$$

$$\tau_3 = -Z_{31}\tau_1 \tag{57}$$

This process reduces the number of unknowns (and linear equations to be solved) from nine to seven.

Table 3 Sphere: effect of ϵ_v on simulation speed and accuracy

ϵ_v	Error in duration of slipping, %	Number of calls
1.0×10^{-1}	4.05	6001
1.0×10^{-2}	0.70	6806
1.0×10^{-3}	0.096	6906
1.0×10^{-4}	0.013	6931
1.0×10^{-5}	0.0017	6961
1.0×10^{-6}	0.00022	6971
1.0×10^{-7}	0.00001	6996

B. Eliminating Constraint Forces During Sticking

Kane's method provides an elegant mechanism[23] for removing Lagrange multipliers, which are also called constraint forces, noncontributing forces, and workless forces. The application of the methodology to the unified friction law is new. The steps required are presented in outline form next. Specific details for carrying out some of the operations described can be found in Ref. 23.

1) Identify dependent and independent generalized speeds. For systems with a few degrees of freedom, it is usually easy to form sets of independent and dependent generalized speeds by inspection. For example, for the rattleback, u_1, u_2, and u_3 can serve as independent generalized speeds, whereas u_4, u_5, and u_6 serve as dependent generalized speeds. A general method for selecting dependent and independent generalized speeds is outlined in Ref. 24.

2) Solve for the time derivatives of the dependent generalized speeds. The time derivatives of the dependent generalized speeds must be expressed as linear combinations of time derivatives of the independent generalized speeds. The equations that govern these relationships can be arrived at in several ways. For example, one may choose to differentiate the velocity-type constraint equations that relate the generalized speeds, e.g., for the rattleback equations (33–47), which resulted from differentiating Eqs. (25–27). Alternately, one may choose to directly form the acceleration-type constraint equations. For the rattleback, this results in $\dot{u}_4$, $\dot{u}_5$, and $\dot{u}_6$ expressed as linear combinations of $\dot{u}_1$, $\dot{u}_2$, and $\dot{u}_3$.

3) Form the constrained dynamic equations from the unconstrained ones. Equations (4.4.3) and (4.11.4) of Ref. (23) provide explicit instructions for reducing a set of n unconstrained dynamic equations of motion containing n time derivatives of generalized speeds and m Lagrange multipliers to a set of $n - m$ constrained dynamic equations of motion that are free of Lagrange multipliers. Subsequent substitution for the time derivatives of the dependent generalized speeds results in a set of $n - m$ equations in $n - m$ unknowns. For the unified friction formulation, this step reduces the work of solving a set of $n + m$ linear equations for n time derivatives of generalized speeds and m Lagrange multipliers to solving a set of $n - m$ linear equations for the $n - m$ time derivatives of independent

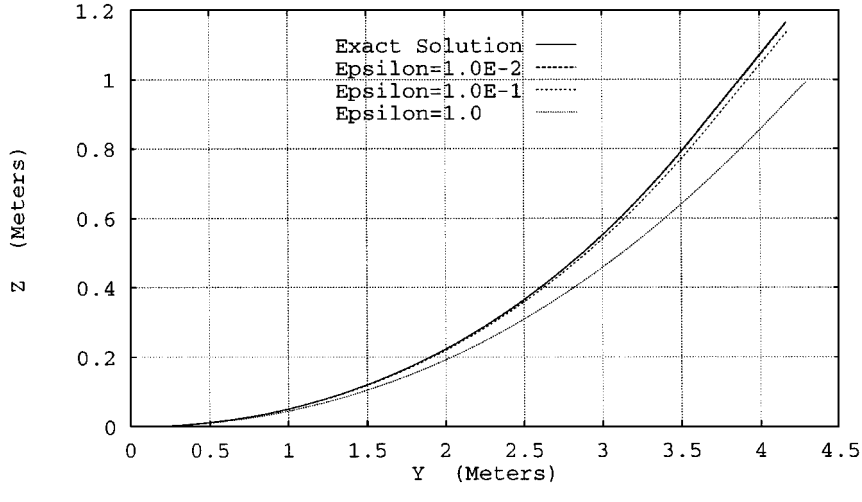

Fig. 11 Motion of contact point of sphere on plane.

generalized speeds. For the rattleback, this process results in a set of dynamic equations governing the values of $\dot{u}_1$, $\dot{u}_2$, and $\dot{u}_3$.

4) Calculate the time derivatives of the dependent generalized speeds. With values for the time derivatives of the independent generalized speeds in hand, the values of the time derivatives of the dependent generalized speeds may be determined from step 2. For the rattleback, this step results in the numerical determination of values for $\dot{u}_4$, $\dot{u}_5$, and $\dot{u}_6$.

5) Solve for the Lagrange multipliers. The m unused dynamic equations of motion may be used to solve for Lagrange multipliers. For the unified friction formulation, these Lagrange multipliers are the normal and friction force measure numbers. For the rattleback, this step results in the numerical determination of values for τ_1, τ_2, and τ_3.

VII. Conclusions

It has been shown that computer simulations of systems with friction can be accurately performed using only the continuous friction law. However, when small values of ϵ_v are employed, the continuous friction law can lead to prohibitively slow and computationally expensive simulations. Improved computational speed and accuracy can be achieved with the unified friction formulation, which requires two switchings to describe the three phases of motion, sticking, slipping, and transition.

References

[1]Baumeister, T., Avallone, E. A., and Baumeister, T., III (eds.), *Marks Mechanical Engineers Handbook*, McGraw–Hill, New York, 1978.

[2]Dahl, P. R., "Solid Friction Damping of Mechanical Vibrations," *AIAA Journal*, Vol. 14, No. 12, 1976, pp. 1675–1682.

[3]Shigley, J. E., and Mishke, C. R., *Mechanical Engineering Design*, McGraw–Hill, New York, 1989, pp. 279–292.

[4]Banerjee, A. K., and Kane, T. R., "Modeling and Simulation of Rotor Bearing Friction," *Journal of Guidance, Control, and Dynamics*, Vol. 17, No. 5, 1994, pp. 1137–1151.

[5]Garcia, A., and Hubbard, M., "Spin Reversal of Rattlebacks: Theory and Experiment," *Proceedings of the Royal Society, Series A: Mathematical and Physical Sciences*, Vol. 418, Feb. 1988, pp. 165–197.

[6]Kane, T. R., and Levinson, D. A., "A Realistic Solution of the Symmetric Top Problem," *Journal of Applied Mechanics*, Vol. 45, No. 4, 1978, pp. 903–909.

[7]Baraff, D., "Coping with Friction for Non-Penetrating Rigid Body Simulation," *Computer Graphics*, Vol. 25, No. 4, 1991, pp. 31–40.

[8]Bondi, H., "The Rigid Body Dynamics of Unidirectional Spin," *Proceedings of the Royal Society, Series A: Mathematical and Physical Sciences*, Vol. 405, 1986, pp. 265–274.

[9]Caughey, T. K., "A Mathematical Model of the Rattleback," *International Journal of Nonlinear Mechanics*, Vol. 15, 1980, pp. 296–302.

[10]Kane, T. R., and Levinson, D. A., "Realistic Mathematical Modeling of the Rattleback," *International Journal of Nonlinear Mechanics*, Vol. 17, No. 3, 1982, pp. 175–186.

[11]Walker, G. T., "On a Dynamical Top," *Quarterly of Pure and Applied Mathematics*, Vol. 28, 1896, pp. 175–184.

[12]Braams, C. M., "On the Influence of Friction on the Motion of a Top," *Physica*, Vol. 18, Nos. 8, 9, 1952, pp. 503–514.

[13]Cohen, R. J., "The Tippe Top Revisited," *American Journal of Physics*, Vol. 45, No. 1, 1977, pp. 12–17.

[14]Fokker, A. D., "The Rising Top, Experimental Evidence and Theory," *Physica*, Vol. 8, No. 6, 1941, pp. 591–596.

[15]Freeman, I. M., "The Tippe Top Again," *American Journal of Physics*, Vol, 24, No. 3, 1956, p. 178.

[16]Gallop, E. G., "On the Rise of a Sleeping Top," *Transactions of the Cambridge Philosophical Society*, Vol. 19, Pt. 3, 1904, pp. 356–373.

[17]Hugenholtz, N. M., "On Tops Rising by Friction," *Physica*, Vol. 18, Nos. 8, 9, 1952, pp. 515–527.

[18]Johnson, F. F., "The Tippy Top," *American Journal of Physics*, Vol, 28, No. 4, 1960, pp. 406–407.

[19]O'Brien, S., and Synge, J. L., "The Instability of the Tippee-Top Explained by Sliding Friction," *Proceedings of the Royal Irish Academy*, Sec. A, Vol. 56, Feb. 1954, pp. 724–728.

[20]Parkyn, D. G., "The Rising of Tops with Rounded Pegs," *Physica*, Vol. 24, 1958, pp. 313–330.

[21]Kane, T. K., *Analytical Elements of Mechanics*, Vol. 2, Stanford Univ. Press, Stanford, CA, 1973, pp. 211–216.

[22]Synge, J. L., and Griffith, B. A., *Principles of Mechanics*, McGraw–Hill, New York, 1949, pp. 447–480.

[23]Kane, T. R., and Levinson, D. A., *Dynamics: Theory and Applications*, McGraw–Hill, New York, 1985, pp. 102–106.

[24]Reckdhal, K. J., "Dynamics and Control of Mechanical Systems Containing Closed Kinematic Chains," Ph.D. Thesis, Dept. of Mechanical Engineering, Stanford Univ., Stanford, CA, Sept. 1996.